Microscopic folding model analysis of the radiative (n,γ) reactions near the $Z = 28$ shell closure and the weak s process

Saumi Dutta,* G. Gangopadhyay,† and Abhijit Bhattacharyya‡
Department of Physics, University of Calcutta, 92 Acharya Prafulla Chandra Road, Kolkata 700009, India
(Received 1 August 2016; revised manuscript received 6 October 2016; published 9 November 2016)

Radiative thermal neutron capture cross sections over the range of thermal energies from 1 keV to 1 MeV are studied in the statistical Hauser-Feshbach formalism. The optical model potential is constructed by folding the density-dependent M3Y nucleon-nucleon interaction with radial matter densities of target nuclei obtained from relativistic-mean-field (RMF) theory. The standard nuclear reaction code TALYS1.8 is used for calculation of cross sections. The nuclei studied in the present work reside near the $Z = 28$ proton shell closure and are of astrophysical interest, taking part in p, s, and r processes of nucleosynthesis. The Maxwellian-averaged cross-section (MACS) values for energies important for astrophysical applications are presented.

DOI: 10.1103/PhysRevC.94.054611

I. INTRODUCTION

After the termination of charged particle induced reactions, the stellar core contains mainly iron and a few trans-iron elements. These elements can act as seeds and take part in further nucleosynthesis by capturing neutrons. Depending upon the conditions of stellar temperature and neutron density, two different nucleosynthesis mechanisms can be possible. The slow neutron capture process or s process, in which, the β-decay rates exceed the neutron capture rates, becomes active at relatively low neutron density and temperature, in which the elements are formed near the valley of β stability. On the other hand, the rapid neutron capture process or r process operates at very high neutron density, in which the neutron capture rates remain very high compared to β-decay rates. A minor contribution comes from a different process, known as the p process, which drives the material through the proton drip line of the nucleosynthesis chart, either by photodisintegration—basically, the (γ,n) reactions—or by capturing protons. The nuclei thus produced are termed p-only nuclei or simply p-nuclei.

Although the majority of the s process theory has been developed, there are still some questions that have to be addressed. The determination of the exact nucleosynthesis path requires a network calculation, the key inputs of which are the thermal neutron capture rates. The s process is subdivided into weak, main, and strong components. The weak component is dominant in the Fe to Sr-Zr-Mo region.

The weak s process, which is responsible for most of the s abundances in the mass region $A = 60$–100, occurs in massive stars ($M \geqslant 8M_{\odot}$, $M_{\odot}$ is the solar mass) [1]. The neutron exposure in massive stars is not too high, hence the local approximation, i.e., $\sigma N_s =$ constant, does not hold well. Hence, the abundance pattern suffers from strong propagation effects for cross-section uncertainties. The uncertainty in the nuclear cross section of a single isotope does not affect the abundance of that particular isotope only, but influences the abundances of subsequent isotopes or the entire distribution. Hence, accurate cross sections are necessary to eliminate the strong propagation effects in the abundance pattern.

The isotopes in the neutron-rich side, those relying on a path outside the s process, are ascribed to the r process and are called r-only nuclei. On the other hand, those which are shielded against the r-process β-decay flow by the stable isobars are produced only in the s process and are termed s-only isotopes. In an explosive r-process scenario, when freeze-out is achieved, the whole material β decays back towards the valley of stability, hence it mixes with the s abundances. Many isotopes have origins from a complex mixture of the p, s, and r processes [2]. The origin of these elements and their formation by different processes in accurate proportion have been studied in recent years. Hence, total (n,γ) cross sections are crucial inputs in this respect.

Some nuclei in this region act as bottlenecks due to their small cross sections. There are a few branchings where the rates of β decay and neutron capture become comparable. Various information regarding stellar conditions during the nucleosynthesis can be drawn from the analyses of branching. For example, one can estimate the neutron density, temperature, electron density, etc., from an accurate analysis of branching. At very high neutron density, many branchings, which in general are not considered in a classical s-process network calculation, can be active. Hence, one has to construct a much larger network in such conditions. In the weak region in massive stars, this process is termed the weak sr process [3]. For example, a significant amount of ^{60}Fe can be produced during the high neutron flux in the shell carbon burning phase of the s process [4]. This is the result of branching at ^{59}Fe with the half-life of 44.495 days. At low neutron densities, neutron capture rate on ^{59}Fe remains lower than the corresponding β-decay rate and the branching does not occur. Thus, one must have complete and proper knowledge of neutron capture cross sections of unstable isotopes in order to study such cases. In such scenarios, theoretical calculations remain the only way to predict the values.

Furthermore, a few isotopes lie in the vicinity of the bridging region of weak and main components of the s process.

*saumidutta89@gmail.com
†ggphy@caluniv.ac.in
‡abhattacharyyacu@gmail.com

Hence, besides their production in the weak s component in massive stars, with masses greater than $8M_{\odot}$, a small fraction of these isotopes are produced in asymptotic giant branch (AGB) stars. For example, the main s process accounts for $\sim$5% of solar copper and $\sim$10% of solar gallium, germanium, and arsenic [5]. Hence, their cross sections are required for the discrimination between the weak and the main s-component contributions.

Precise capture rates have also consequences for r-process study. Once accurate s abundances are obtained, one can easily find abundances of the solar r-process residuals by simply subtracting from the total solar abundance. Some of the isotopes in this region of interest are important for galactic chemical evolution [6]. Some studies have revealed an overabundance problem of certain elements in this region of interest. An explanation of this is hindered due to the limitations in the accurate cross sections. Apart from the astrophysical point of view, the trans-iron elements are also important as structural materials for nuclear reactor applications. Hence, from this perspective also, the neutron cross sections are significant.

We have calculated the radiative thermal neutron capture cross sections for nuclei near the $Z = 28$ proton shell closure from a theoretical viewpoint with the statistical reaction code TALYS1.8 [7]. The aim of our work is to set up a definite and consistent theoretical model that can efficiently predict the cross sections for nuclei over a large mass range as well as energy range for astrophysical applications. This will supplement those cases for which measurement is not possible or not yet done. The paper is organized as follows. In the next section, we briefly describe the theoretical formalism of our work. In Sec. III, we discuss results of the (n,γ) cross sections after comparing them with the available experimental data. Then Maxwellian-averaged cross-section (MACS) values are presented for the nuclei, at an energy of 30 keV. We have also given the MACS values over a range of energies useful for stellar model calculations for a few nuclei which do not have any experimental data. Finally, the summary is presented.

II. THEORETICAL FORMALISM

In the case of neutron-induced reaction, a neutron as a projectile, upon impinging on several target nuclei, results in a binary reaction $A(a,b)B$. The target and the neutron together form a compound nucleus with a total energy $E_{\rm tot} = E_{cm} + S_n + E_x$, and a range of values of spins (J) and parities (π). Here, E_{cm} is the incident energy in the center-of-mass frame, S_n is the neutron separation energy of the compound nucleus, and E_x is the excitation energy of the target which is zero when the target is in the ground state. In the present work, we are studying the radiative neutron capture, i.e., (n,γ) reactions where the compound nucleus, after its formation, decays back to its ground state by emitting subsequent γ rays.

In the very basic sense, the neutron capture cross section $\sigma_{n,\gamma}$, which is a measure of probability of neutron capture, is an effective area that the target presents to the neutron for its absorption, and is defined as the ratio of the number of reactions occurring per unit time per target nucleus to the total incident flux of incoming neutrons. The cross section is dependent on energy of the system and is a sum of the following: a compound nuclear term which is described by the Hauser-Feshbach formula; individual resonances that are determined from the Breight-Wigner formula; the direct capture components that are proportional to $1/v$, v, v^3, etc., for s, p, d waves, respectively, and so on; and, to a certain extent, the interference between direct capture and single resonances. Resonances are observed at low excitation energies when the separation between the levels is large so that the individual peaks appear in the cross section. However, in general, the statistical model calculation of reaction cross sections in the Hauser-Feshbach formalism assumes a large number of resonances at compound formation energies, so that the individual resonances can be averaged over the closely spaced overlapping levels. This cross section is defined as

$$\sigma_{\rm HF} = \sigma_{\rm form}\frac{\Gamma_\gamma}{\Gamma_{\rm tot}}. \tag{1}$$

Here, $\sigma_{\rm form}$ is the formation or the absorption cross section of the compound nucleus, Γ_γ is the partial decay width to the γ channel, and $\Gamma_{\rm tot}$ is the total decay width of all possible exit channels. It is true that the intermediate mass nuclei near the closed shells do not have a high level density, hence most of the statistical model calculation fails near the closed neutron or proton shells. It is our aim to test the validity and reliability of our constructed model in the prediction of reaction cross sections near the magic numbers. The definition of compound nuclear contribution to the total cross section according to the Hauser-Feshbach formula in a compact form can be given as [8]

$$\sigma_{ab} = \frac{\pi}{k_\alpha^2}\sum_{J\pi}\frac{(2J+1)}{(2I_1+1)(2I_2+1)}\frac{T_aT_b}{\sum_c T_c}W_{ab} \tag{2}$$

for each combination of a and b, where the set $a = \{\alpha,l,j\}$ and the set $b = \{\alpha',l',j'\}$. The unprimed and primed quantities are for incident and outgoing channels, respectively. Here, l, s, and j denote the orbital angular momentum, spin, and total angular momentum, respectively, where as α and α' are the channel designators for the projectile + target system and residual nucleus + ejectile system. The average transmission coefficients for incident and outgoing channels are denoted by T_a and T_b while T_c denotes the average transmission coefficients for compound system. I_1 and I_2, are the spins of target and projectile, and J is the total angular momentum of the compound nucleus. At low incident energies (<1 MeV) and for medium mass targets—especially when incident energy is lower than the threshold excitation energy of the first inelastic level—elastic scattering and radiation capture are the dominant processes over inelastic scattering or other reaction channels that gradually open up at higher energies. W_{ab} is the width fluctuation correction factor. These are the crucial renormalization factors to conserve the average cross section. For example, it may be possible that the emission of an ejectile occurs at very early stage of compound nuclear formation before the equilibration or redistribution of energies over all states in the compound system takes place via a sufficient number of collisions. This results in strengthening the elastic scattering channel over the others and a renormalization of each transmission coefficient in the outgoing channel has to

be performed accordingly for the appropriate quantitative description of cross sections. This effect is especially severe near the threshold energies of new channel openings where the channel strengths differ significantly and for low projectile energies when only a few channels exist in the outgoing part.

The entrance channel has neutrons, hence neutron transmission coefficients directly enter into the calculation. These are obtained from a complex optical model potential that can describe the reaction via its imaginary part. The optical model potential describes complicated many-body nucleon-nucleus interaction by an average one-body potential. The wave functions for both elastic scattering and reactions can then be obtained by solving the Schrödinger equation with this complex potential, and then from the phase shifts one can easily determine the transmission coefficients. Thus, the optical model provides the basis for the theoretical calculation of cross sections that can be utilized in various practical applications. Although the earlier approach of a phenomenological potential with a large number of parameters that are adjusted to fit the experimental measurements has been successful, it is limited to only those regions where a sufficient amount of experimental information is available to constrain its parameters. In this regard, recently more accurate microscopic models have been developed by folding the nuclear matter densities with the inherently complicated nucleon-nucleus interaction. The basic advantage of such microscopic models is that they can be reliably applied to regions far from the nuclear stability valley. We have constructed a microscopic neutron optical potential from the density-dependent M3Y (DDM3Y) nucleon-nucleus interaction [9], based on a G-matrix oscillator basis. This interaction is then folded with target radial matter densities, obtained from a relativistic-mean-field (RMF) calculation. The folding is done in coordinate space with spherical symmetry. The folded potential in MeV is given as

$$V_{\rm fold}(\mathbf{r},E) = \int v|(\mathbf{r}-\mathbf{r}',\rho,E)|\rho(\mathbf{r}')d\mathbf{r}'. \tag{3}$$

The interaction $v(\mathbf{r},\rho,E)$ contains two direct terms of different ranges according to the distinct nature of the nuclear force and an energy-dependent zero-range pseudo-potential component representing the exchange term. The interaction in MeV is as follows:

$$v(r,\rho,E) = 2.07\left[7999\frac{e^{-4r}}{4r} - 2134\frac{e^{-2.5r}}{2.5r} - 276\left(1-0.005\frac{E}{A}\right)\delta(r)\right]\left(1-1.624\rho^{\frac{2}{3}}\right). \tag{4}$$

Here, E is the projectile energy in the center-of-mass frame. The folded DDM3Y potential serves as the real part. The optical model potential has been formulated by taking its imaginary part to be identical to the real part, and finally a renormalization has been done by multiplying both the real and imaginary components by numerical factors:

$$V_{\rm omp} = A_r V_{\rm fold} + A_{\rm im} V_{\rm fold}. \tag{5}$$

Earlier, this optical potential was found to describe proton capture reactions over a wide ranges of mass of targets [10–14].

The relativistic-mean-field model, used to obtain baryonic matter density, is based on the "FSU Gold" parametrization [15,16]. The mesonic part of the Lagrangian contains fields for the isoscalar-scalar σ meson, isoscalar-vector ω meson, and isovector-vector ρ meson. Apart from the usual couplings between the nucleon field and meson fields, this RMF model, in addition, contains nonlinear meson self-interaction terms. Pairing is incorporated in the continuum BCS approximation using a delta pairing potential $V(\mathbf{r}_1,\mathbf{r}_2) = -V_0\delta(\mathbf{r}_1-\mathbf{r}_2)$, where the pairing strength V_0 has been chosen to be 300 MeV for both protons and neutrons. The no-sea approximation has been used; i.e., the contribution of baryons from the vacuum has not been considered.

Further, we have convoluted the point proton densities with the standard Gaussian form factor $F(\mathbf{r})$ to obtain the charge distribution and then the root-mean-square (rms) charge radius values in order to check the validity of the RMF model used:

$$\rho_{ch}(\mathbf{r}) = e\int \rho_p(\mathbf{r}')F(\mathbf{r}-\mathbf{r}')d\mathbf{r}', \tag{6}$$

$$F(r) = (a\sqrt{\pi})^{-3}\exp(-r^2/a^2), \tag{7}$$

with $a = \sqrt{2/3}a_p$, where $a_p = 0.80$ fm is the root-mean-square (rms) charge radius of the proton:

$$R_{\rm rms} = \sqrt{\frac{\int r'^2\rho_{ch}(\mathbf{r}')d\mathbf{r}'}{\int \rho_{ch}(\mathbf{r}')d\mathbf{r}'}} \tag{8}$$

The photon transmission coefficient is one of the crucial inputs, as γ transmission is the dominant channel for nuclear deexcitation at energies below a few MeV, especially for neutron-induced reactions. The γ-ray transmission coefficient for multipolarity l and γ-ray energy E_γ for type X [denoting electric (E) or magnetic (M)] is given by

$$T_{Xl}(E_\gamma) = 2\pi f_{Xl}(E_\gamma)E_\gamma^{2l+1}. \tag{9}$$

Obviously, the leading contribution comes from the electric dipole ($l = 1$) transition, for which T_{E1} is essentially proportional to E_γ^3. Since the γ transmission coefficient calculation involves all the possible states to which a photon can be emitted from the initial compound nucleus state, the number of radiative open channels is almost infinite, but each has a very small transmission coefficient. Here, $f_{Xl}(E_\gamma)$ is the energy-dependent γ-ray strength function. Theoretical predictions are necessary due to the incompleteness of the experimental database. There are several methods available for the calculation of the γ-ray strength function. The realistic phenomenological closed form models such as the standard Lorentzian model, the hybrid model, the generalized Fermi liquid model, etc., are gradually replaced by microscopic models that are correlated with nuclear structure properties, due to their superiority in predictive power. Moreover, the phenomenological models suffer from certain severe shortcomings. The predicted values are ambiguous or inappropriate for exotic nuclei and at energies around the neutron separation energy. In our present study, we have taken the values of the $E1$ γ-ray strength function from the microscopic Hartree-Fock-Bogolyubov (HFB) + quasiparticle random phase approximation (QRPA) calculation of Goriely *et al.* [17] from

TABLE I. rms charge radius values, extracted from relativistic-mean-field theory, are compared with the experimental data for the stable nuclei studied in the present work. Experimental values are from Ref. [24].

Nucleus	Charge radius (fm)		Nucleus	Charge radius (fm)	
	Present	Experiment		Present	Experiment
^{56}Fe	3.6936	3.7377	^{57}Fe	3.7073	3.7532
^{58}Fe	3.7211	3.7745	^{59}Co	3.7505	3.7875
^{58}Ni	3.7497	3.7757	^{60}Ni	3.7777	3.8118
^{61}Ni	3.7912	3.8225	^{62}Ni	3.8113	3.8399
^{64}Ni	3.8257	3.8572	^{63}Cu	3.8467	3.8823
^{65}Cu	3.8647	3.9022	^{64}Zn	3.8775	3.9283
^{66}Zn	3.8917	3.9491	^{67}Zn	3.8986	3.9530
^{68}Zn	3.9056	3.9658	^{70}Zn	3.9366	3.9845
^{69}Ga	3.9486	3.9973	^{71}Ga	3.9688	4.0118

drip line to drip line. It takes into account the pairing effects and collective excitations. The QRPA strength was folded with a Lorentzian distribution to generate the experimentally observed GDR widths. The widths were then modified in the framework of a second RPA.

One of the important inputs in statistical calculations are the nuclear level density which is used whenever the information about the discrete level is not available. Nuclear level density (NLD) is the number of nuclear levels per energy interval around an excitation energy, for a certain spin and parity. Experimental information on NLD is limited to only low excitation energies and to those nuclei which are terrestrially accessible for measurement. However, for specific applications, for example in astrophysical studies involving nuclei along neutron or proton drip lines, it is necessary to extrapolate the data, to a large extent, far beyond the experimentally known region. Therefore, for large-scale applications, data have to be taken from reliable theoretical models, as it has been observed that the largest uncertainty in statistical model calculations stems from inappropriate description or prediction of NLDs. Hence, it is of prime interest to choose a physically sound theoretical model. Recently, there have been major improvements in deriving microscopic models over the earlier empirically adjusted phenomenological models. We have taken the data from the recently developed microscopic model of Goriely *et al.* [18] in the combinatorial method including collective rotational and vibrational phonon enhancements to predict spin-, parity-, and energy-dependent NLDs. Goriely *et al.* used the Boson partition function [19], the Hartree-Fock-Bogolyubov ground state properties [20], and the BSk14 interaction [21].

For neutron-induced reactions, the energy range and position of the peak of the distribution are governed by the centrifugal quantum number l; hence, in general, it is determined from the contribution of various partial waves. According to a simple approximation, the peak (E_0) and width (Δ) in MeV are obtained as

$$E_0 = 0.172 T_9 \left(l + \tfrac{1}{2}\right), \tag{10}$$

$$\Delta = 0.194 T_9 \left(l + \tfrac{1}{2}\right)^{\frac{1}{2}}. \tag{11}$$

Hence, for pure s-wave neutron interaction, the peak coincides with that of Maxwell-Boltzmann distribution function.

Neutrons in the interstellar medium are thermalized due to a large number of collisions, and there is obviously a thermal distribution of neutron velocity. It is, therefore, necessary to have the knowledge of average values of cross sections by folding them with a distribution function. In the high-temperature and high-density stellar plasma, quantum effects are negligible, hence the classical Maxwell-Boltzmann (MB) distribution for neutron velocity is a good approximation. The Maxwellian-averaged cross sections (MACS) are obtained by folding the total (n,γ) cross sections with the MB distribution function. These MACS values are generally used in the quantitative calculation of abundances during various phases of evolution of the astrophysical medium. For s-process studies in the classical or canonical scenario, a single MACS at 30 keV is demanded. However, more general network calculations coupled with stellar codes that take into account the temporal evolutionary phases of dense stellar matter require MACS values over a range of neutron energy. Experiments are not possible at all energies, hence theoretical extrapolations are evidently needed. In our earlier studies, this theory was found to be successful in the study of the neutron capture reactions for several nuclei that take part in heavy element nucleosynthesis near the $N = 82$ as well as the $N = 50$ shell closures [16,22]. Some more details on theoretical description are also available there.

III. RESULTS

A. Relativistic-mean-field results

First we present the results of our RMF calculations. In Table I, we have compared rms charge radius values of nuclei in the present study with the measured values. The experimental data are taken from Angeli [24]. Figure 1 shows the radial charge density profiles of some selected nuclei in the region of interest. It can be seen that the RMF theory reproduces the measurements very well.

B. The neutron capture cross sections

Theoretical neutron capture cross sections as a function of neutron energies are compared with existing experimental data

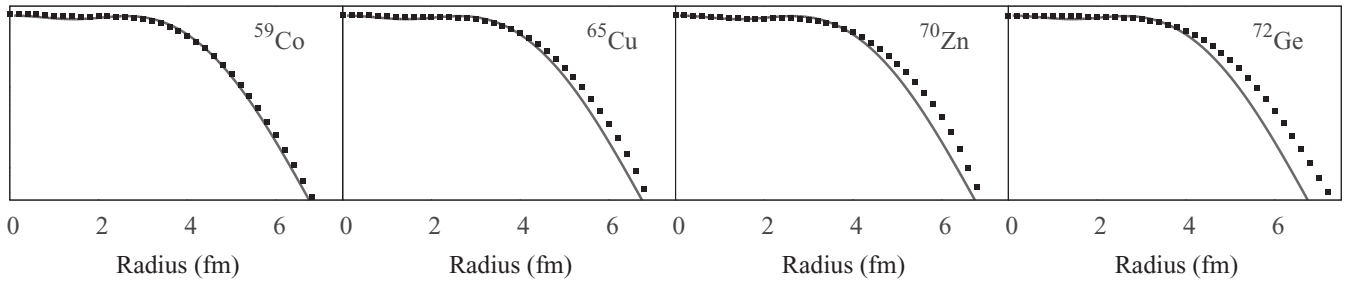

FIG. 1. Charge density profiles of ^{59}Co, ^{65}Cu, ^{70}Zn, and ^{72}Ge, from the relativistic-mean-field theory, are compared with the Fourier-Bessel parameter fit to the elastic electron scattering data, taken from DeVries *et al.* [23]. The solid lines represent theoretical results and the discrete points represent the Fourier-Bessel parameter fit to the scattering data.

in Figs. 3–7. The old measurements, in general, did not have the facilities of modern improved techniques. For example, experiments on ^{66,68}Zn and ^{69}Ga were performed more than 30 years ago. Thus, they suffer from large uncertainties. Recently, Heil *et al.* [25] carried out activation measurements on ^{58}Fe, ^{59}Co, ^{64}Ni, and ^{63,65}Cu with repeated irradiations at a thermal energy of 25 keV. From the neutron spectrum, they finally derived the MACS values after normalizing the measured data with existing differential cross-section values of the data libraries. Furthermore, most of the nuclei in this region have cross sections less than 100 mb. Hence, the smaller the cross sections, the greater is the probability of errors in the measurements, and careful techniques have to be employed. Thus, the impact of the propagation effect is also expected to be more severe over the abundance distribution.

The nucleosynthesis path in the region from Fe to Ga is shown in Fig. 2. The stable and extremely long-lived radionuclides are shown by shaded rectangles. The p-only isotope ^{58}Ni and r-only isotope ^{70}Zn are denoted by rectangles with thick borders.

Figure 3 shows the neutron capture cross sections for $^{56–60}$Fe. The iron nuclei act as seed elements in the s-process nucleosynthesis. The experimental data are from Refs. [4,26–31]. Macklin *et al.* [28] measured the capture cross sections of ^{56,57}Fe from 11 to 60 keV. Later on, Allen *et al.* [26,29] used the time-of-flight (TOF) technique to measure the same from 1 to 800 keV.

Recently, Wang *et al.* [27] measured the energy averaged (n,γ) capture cross sections on ^{56,57}Fe from 15 to 90 keV and 11 to 90 keV, respectively, with an error less than 5%. The energy averaged cross sections on ^{58}Fe measured by Allen and Macklin [31] are extremely scattered and uncertain over the entire range of thermal energies.

The s process on iron elements starts from the most abundant ^{56}Fe and the path uninterruptedly propagates up to ^{59}Fe. The production of ^{60}Fe in the s process is governed by the branching at unstable ^{59}Fe with a β-decay half-life of 44.495 days.

The short-lived radioisotope ^{60}Fe plays the role of an important chronometer for the early solar system (ESS) [32].

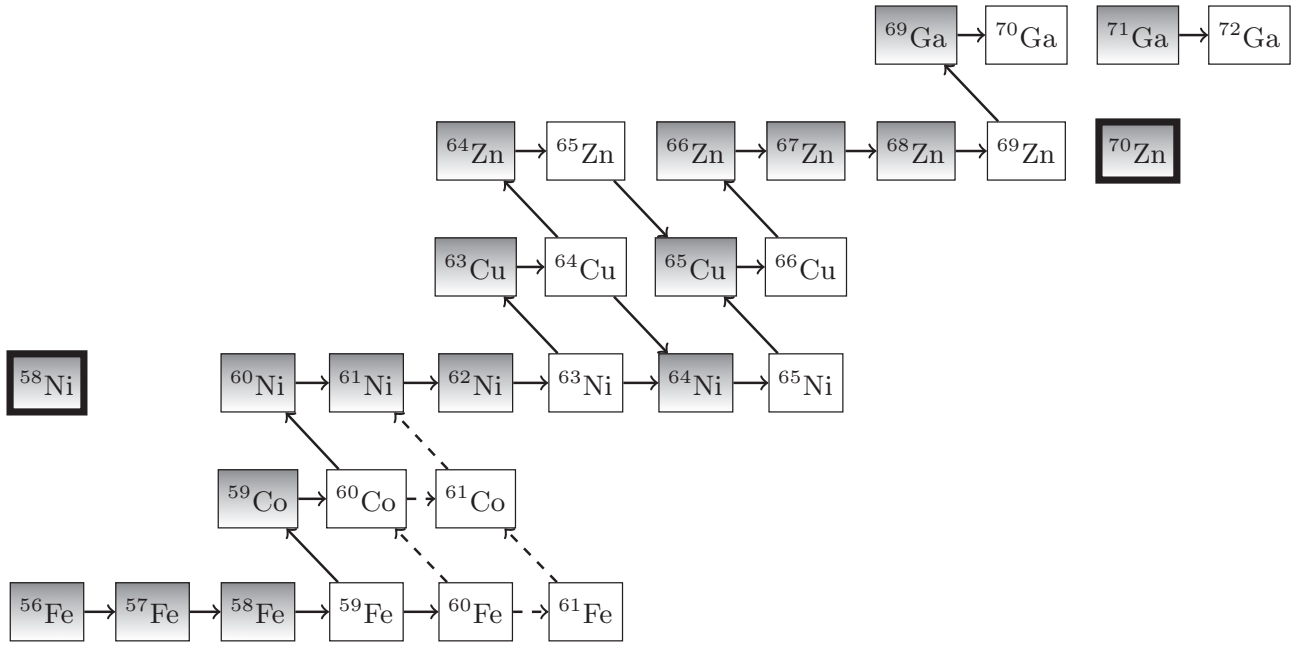

FIG. 2. Nucleosynthesis path from Fe to Ga. Shaded rectangles represent the stable isotopes. The p-only and r-only nuclei are designated by rectangles with thick borders.

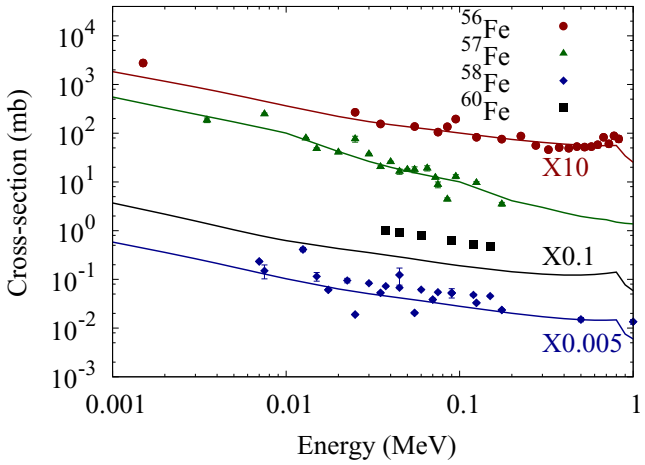

FIG. 3. Comparison of (n,γ) cross sections of the present calculation with experimental measurements for ^{56,57,58,60}Fe. The solid lines indicate the theoretical results. For the convenience of viewing, we have multiplied the cross sections of ^{56,58,60}Fe by factors of 10, 0.005, and 0.1, respectively.

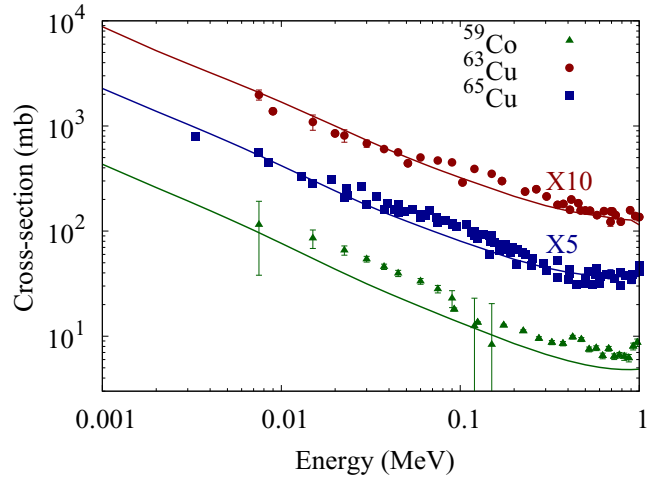

FIG. 4. Comparison of (n,γ) cross sections of the present calculation with experimental measurements for ^{59}Co and ^{63,65}Cu. The solid lines indicate the theoretical results. For the convenience of viewing, we have multiplied the cross sections of ^{63}Cu and ^{65}Cu by factors of 10 and 5, respectively.

The enrichment in ^{60}Ni, in meteoritic inclusions, is evidence of its existence in the ESS [33]. Quitté *et al.* [34] commented that the nucleosynthetic processes (*e* process or *r* process in neutron-rich environments) that generate ^{62}Ni should not also produce ^{60}Ni; hence it can be a result from the decay of ^{60}Fe.

The radioactive decays from ^{60}Co, the daughter of ^{60}Fe, are the proof of its existence in the interstellar medium and also are clear evidence of ongoing neutron capture nucleosynthesis on preexisting stable iron isotopes in massive stars of the Milky Way galaxy [35]. Thus the γ radioactivity of ^{60}Fe, similar to the previously discovered radioactive decay of ^{26}Al (half-life $= 7.2 \times 10^5$ years), can constrain the properties of the interstellar medium [36]. Apart from the study of γ radioactivity, ^{60}Fe(n,γ) cross sections are crucial for the study of its formation procedure in various astrophysical sites, such as supernovae and neutron burst nucleosynthesis.

Uberseder *et al.* [4] did the first experiment on the radiative neutron capture of ^{60}Fe. They used 47 repeated irradiations and found an average experimental value after summing them up. They folded the experimental neutron energy distribution with the differential Hauser-Feshbach statistical model (n,γ) cross sections of Ref. [37] to obtain a normalization factor. This normalized energy differential cross section is then folded with the Maxwell-Boltzmann distribution to obtain the final cross section values for energies ranging from 25 to 100 keV.

Natural cobalt is monoisotopic. The reaction ^{59}Co$(n,\gamma)^{60}$Co is important for nuclear dosimetry applications. It is also used as one of the three most common reaction cross-section standards for the experimental techniques of activation. The radioisotope ^{60}Co is a major neutron activation product of ^{59}Co. The neutron activation cycle requires neutron irradiation without chemical separation, hence monoisotopic ^{59}Co serves as an efficient target. The specific radioactivity of the product is the function of cross sections of both target and product nuclides. Figure 4 shows the total (n,γ) cross sections for ^{59}Co plotted with experimental data, taken from the measurements of Spencer and Macklin [38] and Heil *et al.* [25]. The experiment by Spencer and Macklin [38] was carried out using the TOF technique for thermal energies ranging from 2.5 keV to 1 MeV.

In Figs. 5 and 6, we show the cross sections for $^{58,60-64}$Ni. The experimental values are from Refs. [25,39–48]. Elements of nickel are used as important constituents of structural materials. The isotope ^{58}Ni has its origin only from the *p* process. It is one of the most abundant elements, with an isotopic abundance of 68%, and acts as a seed element

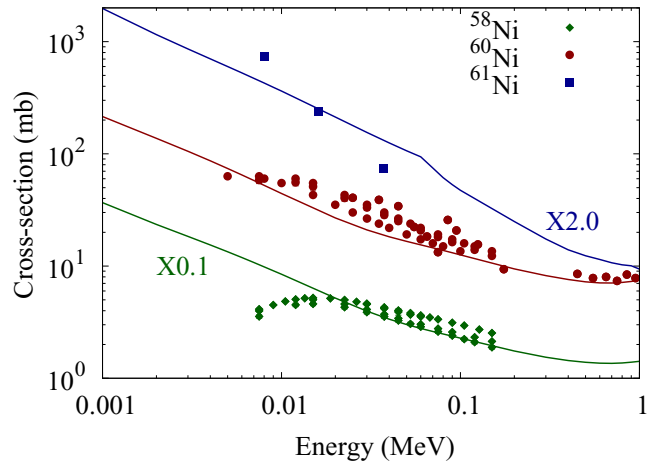

FIG. 5. Comparison of (n,γ) cross sections of the present calculation with experimental measurements for ^{58,60,61}Ni. The solid lines indicate the theoretical results. For the convenience of viewing, we have multiplied the cross sections of ^{58}Ni and ^{61}Ni by factors of 0.1 and 2.0, respectively.

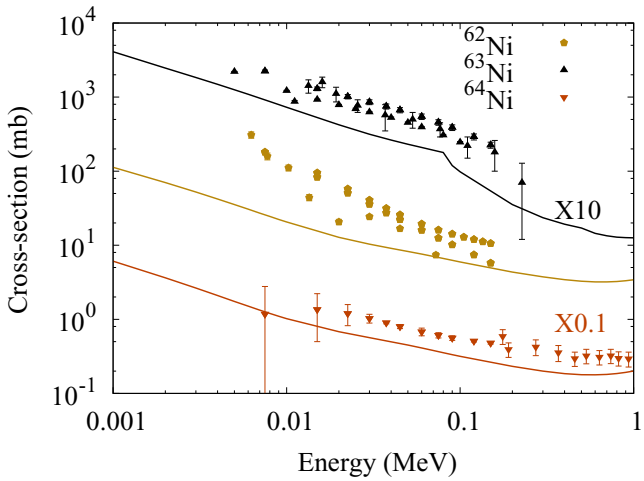

FIG. 6. Comparison of (n,γ) cross sections of the present calculation with experimental measurements for ^{62,63,64}Ni. The solid lines indicate the theoretical results. For the convenience of viewing, we have multiplied the cross sections of ^{63}Ni and ^{64}Ni by factors of 10 and 0.1, respectively.

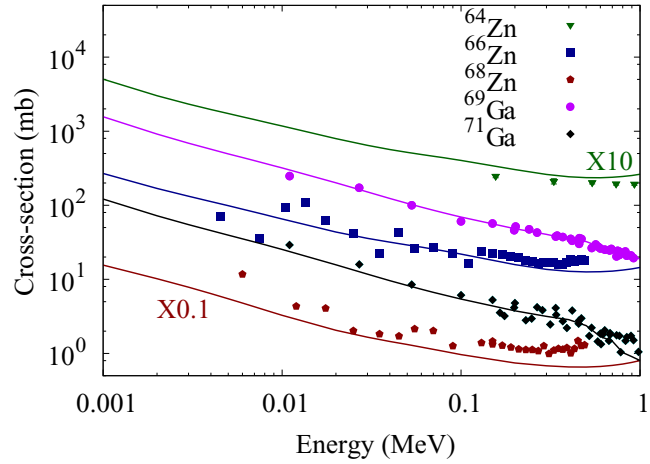

FIG. 7. Comparison of (n,γ) cross sections of the present calculation with experimental measurements for ^{64,66,68}Zn and ^{69,71}Ga. The solid lines indicate the theoretical results. For the convenience of viewing, we have multiplied the cross sections of ^{64}Zn and ^{68}Zn by factors of 10 and 0.1, respectively.

in weak s-process nucleosynthesis. The experimental (n,γ) cross sections of ^{58}Ni are taken from Refs. [39–42]. Perey *et al.* [41] presented both energy-averaged and stellar-averaged cross-section values for ^{58}Ni. The energy averaged cross sections are scattered, hence we have not plotted them. The uncertainties in their measurement are quoted as 15%. There remain sizable differences amongst the existing measurements as well as evaluated results for ^{58}Ni cross sections. Guber *et al.* [42] and Rugel *et al.* [49] reported a global decrease. The most recent measurement by Žugec *et al.* [39] used the n_TOF facility at CERN to measure the cross sections for this isotope. The presence of a significant direct capture component and direct-semidirect capture component, as suggested in Ref. [50], has been investigated in Ref. [42]. However, most of the experiments are unable to separate out these components.

Experimental cross sections are extremely rare for stable ^{61}Ni. We have plotted the data of Tomyo *et al.* [46], who provided experimental values at only three mean energies. We have taken the experimental data of ^{62}Ni from Refs. [46,47,51]. Alpizar-Vicente *et al.* [51] derived the MACS values after normalizing their measured cross sections with those of Sims and Jhunke [52]. Tomyo *et al.* [46] presented average cross sections for this isotope for energies from 5.5 to 90 keV. They further derived the MACS values by normalizing their data with JENDL-3.3 evaluations [53]. The evaluated cross sections of JENDL-3.3 are multiplied by factors of 2 and 1.5, below 5.5 keV and above 90 keV, to derive MACS values. However, our data are found to underpredict all the measurements for ^{62,63}Ni.

The radioactive isotope ^{63}Ni ($t_{1/2} = 101$ years) is an important branch point nucleus, since, at this point, the reaction flow can be diverted towards ^{63}Cu or ^{64}Zn through β decay or towards ^{65}Cu through neutron capture. It is also a long-lived fission product and is used in nuclear transmutation technology. Accurate experimental data are very rare as no natural resource of it is available. We have taken the data from the measurement of Lederer *et al.* [47]. They used the n_TOF facility and determined unresolved cross sections from 10 to 270 keV. The data suffer from a systematic uncertainty of 17%. Our results underproduce the cross-section values by an average factor of $\sim$2 within the given range of thermal energies. We have plotted the data from Refs. [25,48] for ^{64}Ni. Very much earlier than the measurement of Heil *et al.* [25], Grench [48] obtained the neutron capture cross sections relative to gold using the activation technique and compared their results with Hauser-Feshbach statistical model calculations.

The neutron capture cross sections for ^{63,65}Cu are shown with experimental data in Fig. 4. The experimental values are from Refs. [25,54–59]. Recent studies have revealed that a major fraction of the solar copper abundance is produced in massive stars during the s process. However, a contribution is also believed to come from type-Ia supernovae. The element zinc has five stable isotopes. They suffer from large propagation effects in the abundance distribution, mainly because of cross-section uncertainties in ^{63,65}Cu and ^{66,67,68}Zn [25,60]. The isotopes of zinc are also important for the study of galactic chemical evolution. The s-process contribution to isotopes of zinc is lower compared to other trans-iron elements (see Fig. 11 of Ref. [60]). The major fractions of isotopic abundances of ^{64,66}Zn are produced during the α-rich freeze-out in ν winds in massive stars. Bisterzo *et al.* [3] proposed that the weak s process populates mostly the neutron-rich isotopes of zinc. The experimental data for ^{64}Zn and ^{66}Zn are taken from Chen *et al.* [61] and Garg *et al.* [62], respectively, while for ^{68}Zn they are taken from Refs. [63,64]. All these are plotted with our calculated results in Fig. 7.

Spectroscopic observations reveal that most of the gallium abundances are from the s process in massive stars. However, more observational studies are required in order to determine the nucleosynthetic origin of gallium. Gallium has a very low melting point and high boiling point. Hence, it has the largest

TABLE II. Maxwellian averaged cross sections at $kT = 30$ keV for nuclei near the $Z = 28$ shell closure. Experimental values are from Refs. [65,66]. We have also listed theoretical MOST2005 predictions [67]. For unstable and radioactive nuclei, experimental data are not available.

Nucleus	MACS (mb)			Nucleus	MACS (mb)		
	Present	Experiment	MOST		Present	Experiment	MOST
$^{56}_{26}$Fe	19.0	11.7 ± 0.5	36.0	$^{57}_{26}$Fe	32.1	40 ± 4	49.6
$^{58}_{26}$Fe	10.9	13.5 ± 0.7	25.1	$^{59}_{26}$Fe	20.6		
$^{60}_{26}$Fe	3.65	5.15 ± 1.41	6.8				
$^{59}_{27}$Co	33.3	39.6 ± 2.7	53.7	$^{60}_{27}$Co	46.2		
$^{58}_{28}$Ni	42.9	38.7 ± 1.5	72.2	$^{60}_{28}$Ni	23.2	29.9 ± 0.7	39.3
$^{61}_{28}$Ni	77.2	82 ± 8	79.5	$^{62}_{28}$Ni	11.2	22.3 ± 1.6	21.2
$^{63}_{28}$Ni	32.6		42.1	$^{64}_{28}$Ni	5.95	8.0 ± 0.7	10.0
$^{63}_{29}$Cu	76.1	55.6 ± 2.2	146	$^{64}_{29}$Cu	128		
$^{65}_{29}$Cu	37.2	29.8 ± 1.3	48.8				
$^{64}_{30}$Zn	68.8	59 ± 5	90.9	$^{65}_{30}$Zn	250		260
$^{66}_{30}$Zn	38.1	35 ± 3	51.0	$^{67}_{30}$Zn	153	153 ± 15	174
$^{68}_{30}$Zn	17.9	19.2 ± 2.4	20.9	$^{70}_{30}$Zn	6.03		10.1
$^{69}_{31}$Ga	152	139 ± 6	122	$^{71}_{31}$Ga	121	123 ± 8	117

liquid range of any metal. Apart from the astrophysical point of view, it is a promising candidate in reactor technology for liquid metallic coolant [68]. Nowadays reliable cross sections are also in great demand to study the interaction of gallium with neutrons [69]. The thermal neutron capture cross sections are taken from Refs. [70–72]. The experimental data are extremely old. They were measured more than 30 years ago. We have plotted the data with our theoretical results in Fig. 7.

C. Maxwellian-averaged cross section (MACS) values

In Table II, we have presented the MACS values at 30 keV for the nuclei shown in the reaction path (Fig. 2). They are listed with the available experimental values taken from the KADoNiS database [66], which is an updated version of recommended values by Bao *et al.* [65]. For the sake of comparison, we have also listed the theoretical MOST2005 calculations [67], whenever available. It can be seen that our theory reproduces the experimental values better than MOST2005 calculations, except for a few cases.

There are discrepancies in the MACS values of ^{62}Ni. The direct neutron capture cross section in the distorted-wave Born approximation (DWBA) calculation by Rauscher and Guber [73] confirmed that there are contributions from subthreshold resonance and p-wave capture. However, thereafter Tomyo *et al.* [46] refused any p-wave contribution in their measurement. They presented a much larger MACS of 37 ± 3.2 mb at 30 keV and claimed that this new large value may solve the longstanding overproduction problem of ^{62}Ni abundance.

In Table III, we present the Maxwellian-averaged cross sections from 5 to 100 keV for the nuclei ^{59}Fe, ^{60}Co, and ^{63}Ni. Experimental data are not available for these nuclei. These isotopes are unstable, hence they are not available for measurement. The isotopes ^{59}Fe and ^{60}Co may be subject to the weak *sr* process [3] in massive stars where they can act as important branch points. Hence, their MACS values would be needed in a complete network calculation to determine the abundances in such astrophysical sites with high neutron density and temperature. The isotope ^{63}Ni is an important and strong branch-point nucleus, as discussed above.

TABLE III. Theoretical MACS values (mb) over a range of energy for reactions with unstable targets ^{59}Fe, ^{60}Co, and ^{63}Ni. Experimental values are not available for these nuclei.

kT (MeV)	0.005	0.010	0.015	0.020	0.025	0.030	0.040	0.050	0.060	0.080	0.100
^{59}Fe	81.5	47.0	34.3	27.7	23.5	20.6	16.8	14.4	12.7	10.5	9.1
^{60}Co	178	105	77.7	62.6	53.0	46.2	37.2	31.4	27.2	21.7	18.2
^{63}Ni	127	74	55	44	38	33	26	21	18	13	11

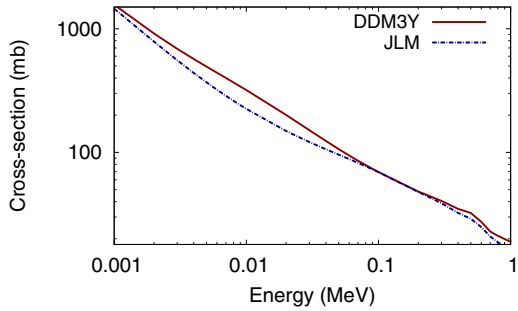

FIG. 8. Predicted cross section values for ^{69}Ga$(n,\gamma)^{70}$Ga reaction with two different density-folded microscopic potentials based on two different nucleon-nucleus interactions. The red solid line represents a calculation with optical model potential based on the DDM3Y *NN* interaction and the blue dotted line represents calculations with the JLM optical model potential.

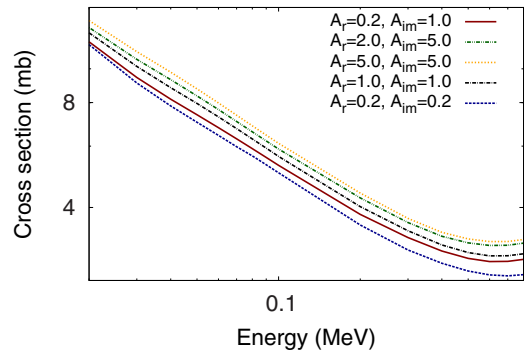

FIG. 9. Cross sections for the reaction ^{58}Fe$(n,\gamma)^{59}$Fe with different combinations of real and imaginary potential well depths.

IV. SENSITIVITY TO THE NEUTRON OPTICAL POTENTIAL

According to the Hauser-Feshbach theory of compound nuclear reactions, the total cross section $\sigma_{\rm tot} = \frac{T_n T_\gamma}{T_{\rm tot}}$. The transmission coefficients (T) are linearly proportional to average channel widths, hence $\sigma_{\rm tot} \propto \frac{\Gamma_n \Gamma_\gamma}{\Gamma_{\rm tot}}$. For radiative capture reactions at low energy and for intermediate mass nuclei, the average neutron width is much greater than the average radiation width, hence the resonances in radiative neutron capture are always accompanied with potential elastic scattering. In such a case, $\sigma_{\rm tot}$ would, in principle, be predominantly proportional to Γ_γ. Hence, to verify whether the Hauser-Feshbach cross sections depend on the choice of neutron optical potential, we have performed the calculations with a different neutron optical potential based on the Jeukene-Lejuene-Mahaux (JLM) interaction [74]. The other input parameters such as level density, $E1$ γ-ray strength function, etc., have been taken from the same references as in the case of calculations with our potential based on the M3Y interaction.

The JLM potential for a given nuclear matter density $\rho_m = \rho_n + \rho_p$ and asymmetry $\alpha = \frac{\rho_n - \rho_p}{\rho}$ has been obtained by folding the nuclear matter density distribution with Reid's hard core nucleon-nucleon interaction:

$$U_{NM}(E)_{\rho\alpha} = \lambda_V(E)[V_0(E) + \lambda_{V1}\alpha V1(E)] + i\lambda_W(E)[W_0(E) + \lambda_{W1}\alpha W1(E)]. \quad (12)$$

Where, λ_V, λ_{V1}, λ_W, and λ_{W1} are real and imaginary isoscalar and isovector components [74]. The final form of the JLM potential considering the local density approximation for the application to finite nuclei is given as

$$U_{FN} = (t\sqrt{\pi})^{-3} \int \frac{U_{NM}(\rho(r'),E)}{\rho(r')} \exp\left(-\frac{|\mathbf{r}-\mathbf{r}'|^2}{t_r^2}\right)\rho(r')d\mathbf{r}'. \quad (13)$$

Due to the limitation of the length of the paper, we have shown the comparison between two potentials only for the ^{69}Ga$(n,\gamma)^{70}$Ga reaction in Fig. 8. Two potentials give different results for cross-section values. Our microscopic potential has also been found to predict results different from the JLM potential in our earlier studies near the $N = 82$ and the $N = 50$ closed neutron core [16,22]. This suggests that the statistical model calculations of (n,γ) cross sections are indeed sensitive to the neutron optical potential.

Further, in order to check the sensitivity to the parameters A_r and $A_{\rm im}$ in Eq. (5), we have varied the depths of the potential for both real and imaginary components by various factors and observed changes in cross section values by different percentages depending upon the reactions concerned. In Fig. 9, we have shown the results for the target ^{58}Fe for a number of combinations of depth parameters. The depths of real and imaginary parts of the complex potential have been increased and decreased to several factors of their unnormalized values and the enhanced or reduced cross section values are plotted with the cross sections obtained with unnormalized depths. The other reactions more or less follow the same trend.

It is, therefore, obvious that by properly tuning these parameters for each individual reaction, one can achieve better agreement with experimental values. Nevertheless, it is evident from Figs. 3–7 and from presented values in Table II that the cross sections can be reasonably described with unnormalized potential depths. This was also the case in our previous studies [16,22]. Moreover, it is convenient to establish a uniquely parameterized potential model instead of an individual fit, as it can reflect a more general and global behavior. A further advantage of a single parameter set is that the model can subsequently be applied to predict the cross-section values that are unknown or yet to be measured.

V. SUMMARY

To summarize, we have performed statistical model Hauser-Feshbach calculations in a microscopic approach to derive the radiative neutron capture cross sections for nuclei in the vicinity of the $Z = 28$ proton shell. The nuclei are of astrophysical interest, taking part in the weak component of the s process, occurring in massive stars, and also in the p and r processes. The RMF theory is employed to extract target radial densities to use in folding the DDM3Y *NN* interaction. The (n,γ) cross sections are compared with available experimental

data and reasonable agreements are achieved for almost all of the nuclei. This ensures the feasibility of our theoretical statistical model to predict the radiative thermal capture cross sections, even in the regions where only a few or even no experimental data exist. The Maxwellian-averaged cross sections relevant to astrophysical applications are presented.

ACKNOWLEDGMENTS

The authors acknowledge financial assistance from the University Grants Commission of India (Junior Research Fellowship and Departmental Research Scheme) and from the Alexander von Humboldt Foundation.

[1] J. G. Peters, Astrophys. J. **154**, 225 (1968).
[2] K. Farouqi, K.-L. Kratz, and B. Pfeiffer, Pub. Astron. Soc. Aust. **26**, 194 (2009).
[3] S. Bisterzo, R. Gallino, M. Pignatari, L. Pompeia, K. Cunha, and V. Smith, Mem. Soc. Astron. Ital. **75**, 741 (2004).
[4] E. Uberseder, R. Reifarth, D. Schumann, I. Dillmann, C. D. Pardo, J. Gorres, M. Heil, F. Kappeler, J. Marganiec, J. Neuhausen, M. Pignatari, F. Voss, S. Walter, and M. Wiescher, Phys. Rev. Lett. **102**, 151101 (2009).
[5] S. Randich and L. Pasquini, in *Chemical Abundances and Mixing in Stars in the Milky Way and its Satellites: Proceedings of the ESO-Arcetric Workshop, September 13–17, 2004, Castiglione della Pescaia, Italy* (Springer-Verlag, Berlin, 2006).
[6] A. Alibès, J. Labay, and R. Canal, Astron. Astrophys. **370**, 1103 (2001).
[7] A. J. Koning, S. Hilaire, and M. Duizvestijn, in *Proceedings of the International Conference on Nuclear Data for Science and Technology, April 22–27, 2007, Nice, France*, edited by O. Bersillon, F. Gunsing, E. Bauge, R. Jacqmin, and S. Leray (EDP Sciences, Les Ulis, France, 2008), p. 211; www.talys.eu.
[8] See, for example, C. Iliadis, *Nuclear Physics of Stars* (Wiley-VCH, Weinheim, Germany, 2007).
[9] A. M. Kobos, B. A. Brown, P. E. Hodgson, G. R. Satchler, and A. Budzanowski, Nucl. Phys. A **384**, 65 (1982).
[10] S. Dutta, D. Chakraborty, G. Gangopadhyay, and A. Bhattacharyya, Phys. Rev. C **91**, 025804 (2015).
[11] C. Lahiri and G. Gangopadhyay, Eur. Phys. J. A **47**, 87 (2011).
[12] C. Lahiri and G. Gangopadhyay, Phys. Rev. C **84**, 057601 (2011).
[13] D. Chakraborty, S. Dutta, G. Gangopadhyay, and A. Bhattacharyya, Phys. Rev. C **91**, 057602 (2015).
[14] D. Chakraborty, S. Dutta, G. Gangopadhyay, and A. Bhattacharyya, Phys. Rev. C **94**, 015802 (2016).
[15] B. G. Todd-Rutel and J. Piekarewicz, Phys. Rev. Lett. **95**, 122501 (2005).
[16] S. Dutta, D. Chakraborty, G. Gangopadhyay, and A. Bhattacharyya, Phys. Rev. C **93**, 024602 (2016).
[17] S. Goriely, E. Khan, and M. Samyn, Nucl. Phys. A **739**, 331 (2004).
[18] S. Goriely, S. Hilaire, and A. J. Koning, Phys. Rev. C **78**, 064307 (2008).
[19] S. Hilaire, J. P. Delaroche, and M. Girod, Eur. Phys. J. A **12**, 169 (2001).
[20] S. Goriely, M. Samyn, and J. M. Pearson, Phys. Rev. C **75**, 064312 (2007).
[21] S. Hilaire and S. Goriely, Nucl. Phys. A **779**, 63 (2006).
[22] S. Dutta, G. Gangopadhyay, and A. Bhattacharyya, Phys. Rev. C **94**, 024604 (2016).
[23] H. DeVries, C. W. DeJager, and C. DeVries, At. Data Nucl. Data Tables **36**, 495 (1987).
[24] I. Angeli, At. Data Nucl. Data Tables **87**, 185 (2004).
[25] M. Heil, F. Käppeler, E. Uberseder, R. Gallino, and M. Pignatari, Phys. Rev. C **77**, 015808 (2008).
[26] B. J. Allen, A. R. de L. Musgrove, J. W. Boldeman, M. J. Kenny, and R. L. Macklin, Nucl. Phys. A **269**, 408 (1976).
[27] T. Wang, M. Lee, G. Kim, Y. Oh, W. Namkung, T.-I. Ro, Y.-R. Kang, M. Igashira, and T. Katabuchi, Nucl. Instrum. Methods Phys. Res. B **268**, 440 (2010).
[28] R. L. Macklin, P. J. Pasma, and J. H. Gibbons, Phys. Rev. **136**, B695 (1964).
[29] B. J. Allen, A. R. de L. Musgrove, R. Taylor, and R. L. Macklin, in *Neutron Data of Structural Materials for Fast Reactors*, Proceedings of a Specialists' Meeting Held at the Central Bureau for Nuclear Measurements, December 5–8, 1977, Geel, Belgium, edited by K. H. Böckhoff (Oxford University Press, New York, 1978), p. 476.
[30] Yu. N. Trofimov, At. Energ. **58**, 278 (1985).
[31] B. J. Allen and R. L. Macklin, J. Phys. G: Nucl. Part. Phys. **6**, 381 (1980).
[32] A. Boss, Astrophys. J. **660**, 1707 (2007).
[33] J. Birck and G. Lugmair, Earth Planet. Sci. Lett. **90**, 131 (1988).
[34] G. Quitté, A. N. Halliday, B. S. Meyer, and A. Markowski, Astrophys. J. **655**, 678 (2007).
[35] G. Rugel, T. Faestermann, K. Knie, G. Korschinek, M. Poutivtsev, D. Schumann, N. Kivel, I. Gunther-Leopold, R. Weinreich, and M. Wohlmuther, Phys. Rev. Lett. **103**, 072502 (2009).
[36] R. Diehl, N. Prantzos, and P. von Ballmoos, Nucl. Phys. A **777**, 70 (2006).
[37] T. Rauscher and F.-K. Thielemann, At. Data Nucl. Data Tables **75**, 1 (2000).
[38] R. R. Spencer and R. L. Macklin, Nucl. Sci. Eng. **61**, 346 (1976).
[39] P. Žugec, Phys. Rev. C **89**, 014605 (2014).
[40] K. Wisshak, F. Käppeler, G. Reffo, and F. Fabbri, Nucl. Sci. Eng. **86**, 168 (1984).
[41] C. M. Perey, J. A. Harvey, R. L. Macklin, R. R. Winters, and F. G. Perey, Oak Ridge National Laboratory Report No. 5893, 1982 (unpublished).
[42] K. H. Guber, H. Derrien, L. C. Leal, G. Arbanas, D. Wiarda, P. E. Koehler, and J. A. Harvey, Phys. Rev. C **82**, 057601 (2010).
[43] R. G. Stieglitz, R. W. Hockenbury, and R. C. Block, Nucl. Phys. A **163**, 592 (1971).
[44] C. M. Perey, J. A. Harvey, R. L. Macklin, R. R. Winters, and F. G. Perey, Oak Ridge National Laboratory Report No. 5893, 1982 (unpublished).
[45] F. Corvi, G. Fioni, F. Gunsing, P. Mutti, and L. Zanini, Nucl. Phys. A **697**, 581 (2002).
[46] A. Tomyo, Y. Temma, M. Segawa, Y. Nagai, H. Makii, T. Shima, T. Ohsaki, and M. Igashira, Astrophys. J. **623**, L153 (2005).

[47] C. Lederer *et al.*, Phys. Rev. C **89**, 025810 (2014).
[48] H. A. Grench, Phys. Rev. **140**, B1277 (1965).
[49] G. Rugel, I. Dillmann, T. Faestermann *et al.*, Nucl. Instrum. Methods B **259**, 683 (2007).
[50] W. E. Parker, M. B. Chadwick, F. S. Dietrich *et al.*, Phys. Rev. C **52**, 252 (1995).
[51] A. M. Alpizar-Vicente, T. A. Bredeweg, E.-I. Esch, U. Greife, R. C. Haight, R. Hatarik, J. M. O'Donnell, R. Reifarth, R. S. Rundberg, J. L. Ullmann, D. J. Vieira, and J. M. Wouters, Phys. Rev. C **77**, 015806 (2008).
[52] G. H. E. Sims and D. G. Juhnke, J. Inorg. Nucl. Chem. **32**, 411 (1970).
[53] K. Shibata *et al.*, J. Nucl. Sci. Technol. **39**, 1125 (2002); http://wwwndc.jaea.go.jp/jendl/j33/j33.html.
[54] V. A. Tolstikov, V. P. Koroleva, V. E. Kolesov, and A. G. Dovbenko, At. Energ. **21**, 45 (1966).
[55] G. G. Zaikin, I. A. Korzh, N. T. Sklyar, and I. A. Totskii, Sov. At. Energy **25**, 1362 (1968).
[56] J. M. Blair, M. Deutsch, K. M. Griesen, A. O. Hanson, G. A. Linenberger, J. A. Miskel, R. F. Taschek, C. M. Turner, and J. H. Williams, Los Alamos National Laboratory Report No. 95, 1944 (unpublished).
[57] V. A. Tolstikov, V. E. Kolesov, A. G. Dovbenko, and Ju. Ja. Stavisskij, At. Energ. **17**, 505 (1964).
[58] Yu. Ya. Stavisskiy and V. A. Tolstikov, At. Energ. **10**, 508 (1961).
[59] A. E. Johnsrud, M. G. Silbert, and H. H. Barschall, Phys. Rev. **116**, 927 (1959).
[60] M. Pignatari, R. Gallino, M. Heil, M. Weischer, F. Käppeler, F. Herwig, and S. Bisterzo, Astrophys. J. **710**, 1557 (2010).
[61] J.-X. Chen, Z.-M. Shi, G.-Y. Tang, and G.-H. Zhang, Chin. J. Nucl. Phys. (Beijing) **17**, 342 (1995).
[62] J. B. Garg, V. K. Tikku, J. A. Harvey, R. L. Macklin, and J. Halperin, Phys. Rev. C **24**, 1922 (1981).
[63] J. B. Garg, V. K. Tikku, J. A. Harvey, J. Halperin, and R. L. Macklin, Phys. Rev. C **25**, 1808 (1982).
[64] A. I. Leipunskiy, O. D. Kazachkovskiy, G. Ja. Artyukhov, A. I. Baryshnikov, T. S. Belanova, V. I. Galkov, Yu. Ja. Stavisskiy, E. A. Stumbur, and L. E. Sherman, in *Proceedings of the Second United Nations Conference on the Peaceful Uses of Atomic Energy, September 1–13, 1958, Geneva* (United Nations, Geneva, 1958), Vol. 15, p. 50.
[65] Z. Y. Bao, H. Beer, F. Käappeler, F. Voss, and K. Wisshak, At. Data Nucl. Data Tables **76**, 70 (2000).
[66] I. Dillmann, R. Plag, F. Käppeler, and T. Rauscher, in *EFNUDAT Fast Neutrons, Proceedings of the Scientific Workshop on Neutron Measurements, Theory, and Applications, April 28–30, 2009, Geel, Belgium*, edited by F.-J. Hambsch (Publications Office of the European Union, Luxembourg, 2010), p. 55; www.kadonis.org.
[67] M. Arnould and S. Goriely, Phys. Rep. **384**, 1 (2003).
[68] T. Sawada, A. Netchaev, H. Ninokata, and H. Endo, Prog. Nucl. Energy **37**, 313 (2000).
[69] L. Koester, K. Knopf, W. Waschkowski, and A. Klüver, Z. Phys. A **318**, 347 (1984).
[70] A. G. Dovbenko, V. E. Kolesov, V. P. Koroleva, and V. A. Tolstikov, Sov. At. Energy **26**, 82 (1969).
[71] G. G. Zaikin, I. A. Korzh, M. V. Pasechnic, and N. T. Skljar, Ukr. Fiz. Zh. **16**, 1205 (1971).
[72] Yu. Ya. Stavisskii and V. A. Tolstikov, At. Energ. **7**, 259 (1959).
[73] T. Rauscher and K. H. Guber, Phys. Rev. C **66**, 028802 (2002); **71**, 059903(E) (2005).
[74] E. Bauge, J. P. Delaroche, and M. Girod, Phys. Rev. C **63**, 024607 (2001).